Concentration, temperature, and *p*H dependence of sunset-yellow aggregates in aqueous solutions: An x-ray investigation

Leela Joshi,[1] Shin-Woong Kang,[2] Dena Mae Agra-Kooijman,[1] and Satyendra Kumar[1]
[1]*Department of Physics, Kent State University, Kent, Ohio 44242, USA*
[2]*Department of BIN Fusion Technology, Chonbuk National University, Jeonju, South Korea 561-756*
(Received 19 May 2009; published 7 October 2009)

The dye sunset yellow (SY) forms columnar aggregates via π-π stacking in aqueous solutions. These aggregates develop orientational and translational order at elevated concentrations to exhibit the nematic (N) and columnar (C) mesophases. Positional-order correlation lengths of the aggregates in the directions parallel and perpendicular to the stacking direction were measured as functions of temperature, concentration, and ionic content of solutions with synchrotron x-ray scattering in magnetically aligned samples. Average length of aggregates (i.e., the number of SY molecules in an aggregate) grows monotonically with concentration while their effective transverse separation decreases. The scission energy, E, determined from the Arrhenius thermal evolution of the longitudinal correlation length, is found to be $4.3 \pm 0.3\ k_BT$ and $3.5 \pm 0.2\ k_BT$, in the N and C phases, respectively. Temperature and concentration dependence of E suggests that chromonic aggregation is not an isodesmic process. The aggregate length decreases with decreasing *p*H when HCl is added to the solution.

DOI: 10.1103/PhysRevE.80.041703 PACS number(s): 61.30.Eb, 42.70.Df, 61.30.St, 64.70.M−

I. INTRODUCTION

Liquid crystal phases formed by aqueous solutions of dye and drug compounds were established long time ago [1–4]. These are termed as lyotropic chromonic liquid crystals (LCLCs). The materials that form the LCLC phases generally have planklike molecules with polyaromatic cores surrounded by hydrophilic ionic groups at the periphery. When dissolved in water, they undergo self-assembly due to π-π interaction between their cores to form stacks (or, aggregates) which act as building blocks of the mesophase. The length of the aggregates increases with dye concentration. At high enough dye concentrations, the organization of the aggregates typically leads to the formation of two liquid crystal phases, nematic (N) and columnar (C). Previous studies [2–5] suggest that in chromonic self-assemblies, entropic driving forces are smaller than enthalpy forces based on π-π interaction between aromatic cores. Other factors that play important roles in the aggregation process of dye molecules [6–8] include: electrostatic repulsion between ionic groups such as sulfonate in sunset yellow (SY), interaggregate interactions controlled by excluded volume effect, electrostatic forces between surface charges of aggregates and counter ions in the solution, and hydration forces [9]. Our understanding of the microscopic structure and the behavior of molecular aggregates in different phases remains incomplete. Some experimental results [1,5,7] suggest the formation of stacking of single planklike objects while others suggest the formation of hollow columns [10] with four dye molecules in a plane perpendicular to the aggregate axis and resembling a chimney.

To obtain a deeper insight into the structure of the aggregates and LCLC phases of SY, we studied the effect of changes in dye concentration, ionic additives, and temperature using x-ray diffraction and polarizing microscopy. In addition to the structural parameters, we determined the positional-order correlation lengths in the directions longitudinal and transverse to the aggregate axis. In this paper, we describe experimental results that show how the inter- and intra-aggregate spacings change with concentration and temperature. From temperature-induced changes in the longitudinal correlation length in the N and C phases, the scission energy, i.e., the energy needed to break one aggregate into two, is estimated.

II. EXPERIMENTAL DETAILS

Molecular structure of sunset yellow both in NH hydrazone and OH azo tautomer are shown in Fig. 1. The azo form [Fig. 1(a)] consists of two rigid aromatic chromophores connected by an azo, N=N, bridge with water-solubilizing groups at the periphery, whereas, in the hydrazone form [Fig.

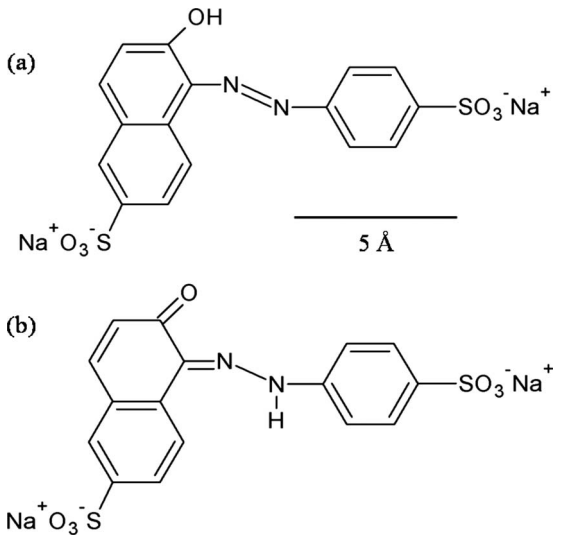

FIG. 1. Molecular structure of sunset yellow dye: (a) azo tautomer with scale bar (b) NH hydrazone tautomer.

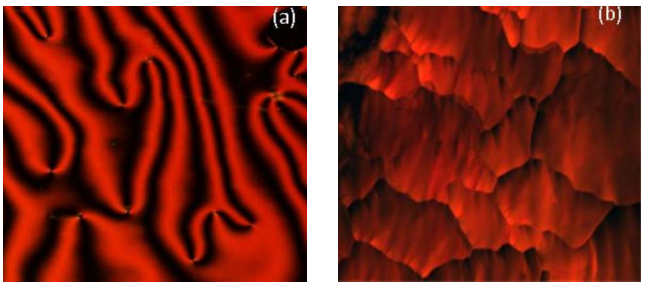

FIG. 2. (Color online) Optical textures of sunset yellow solutions in the (a) nematic (30 wt % solution), and (b) columnar phase (40 wt % solution) at room temperature.

1(b)], the hydrogen resides on the distant nitrogen of the azo bond. Edwards *et al.* [5] have shown that the hydrazone tautomer is present in all phases of solutions of SY. Samples of 90% pure SY were purchased from Sigma-Aldrich and were purified by recrystallization from solutions in high pressure liquid chromatography (HPLC) grade ethanol and water purchased from Fisher Scientific. The recrystallization and filtration processes were repeated once again. The precipitates were filtered and dried in vacuum for 48 h at 110 °C [4].

To identify the LC phases, optical textures of dye solutions were captured using an Olympus BX51 polarizing optical microscope connected to an Olympus U-CMAD3 camera. Sandwich cells were made with glass plates using 10 μm thick Mylar strips as spacers. Immediately after filling, the cells were sealed with 5 min epoxy to prevent water evaporation. Representative optical textures of the N and C phases of the SY+water solutions are shown in Fig. 2. Changes in the optical textures were used to obtain the temperature-concentration phase diagrams of the SY solutions with and without HCl. The aqueous solutions of sunset yellow with HCl were prepared by calculating the ratio of the number of moles of SY to hydrochloric acid, represented as SY: HCl, keeping SY concentration the same. The results are summarized in Fig. 3. Sample temperature was changed, during heating and cooling, at a rate of 0.4 °C/min. The phase diagram includes a wide (10–12 °C) biphasic region in which the N and isotropic (I) phases coexist. The addition of HCl lowers the temperatures at which the biphasic region I+N begins and ends, as shown in this figure.

For x-ray diffraction, the SY solutions were filled in 1.5 mm diameter Lindèman capillaries that were subsequently flame-sealed. Temperature of the sample was controlled with a precision of ±0.1 °C using an INSTEC hot stage. A pair of rare-earth permanent magnets placed inside the hot-stage helped in aligning the long axis of the aggregates and, thus, the nematic director. Dye molecules have positive diamagnetic anisotropy and orient parallel to the magnetic field. Consequently, the aggregate axes and thus the nematic director lie in the plane perpendicular to the magnetic field. The degree of macroscopic alignment of a nematic typically depends on the field strength and diamagnetic anisotropy of the aggregates, which will vary with concentration and temperature. However, we do not calculate or use the degree of alignment in any of our conclusions. High-resolution x-ray diffraction experiments were performed at the Midwestern Universities Collaborative Access Team's sector No.

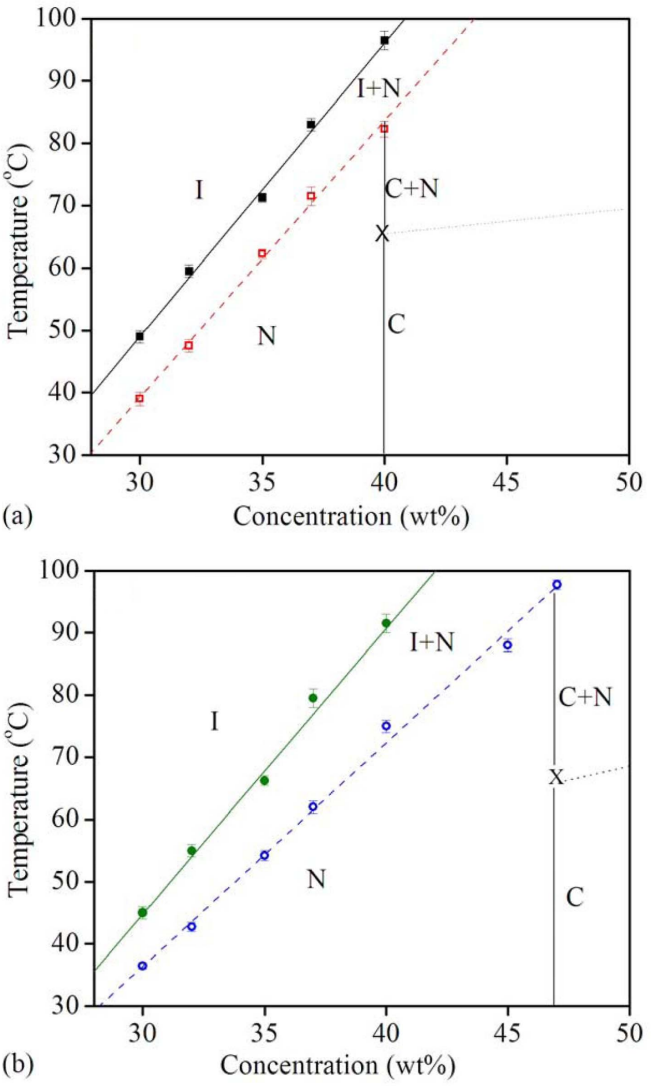

FIG. 3. (Color online) Phase diagram of aqueous solutions of (a) sunset tellow and (b) sunset yellow and HCl in 1:1 mol ratio.

6 of the Advance Photon Source at Argonne National Laboratory using a wavelength of 0.765 34Å. The diffraction patterns were recorded using a high-resolution image-plate detector (MAR345) placed at a distance of 518.5 mm from the sample. The data were calibrated against a silicon standard traceable to the National Institute of Standards and Technology.

X-ray diffraction patterns of the nematic and columnar phases typically consisted of two sets of reflections in mutually orthogonal directions. Additionally, four faint diffuse spots were also present at intermediate angles, corresponding to a *d*-spacing of 5.6 Å. From the data analysis, we obtained the temperature dependence of the aggregate dimensions and the two correlation lengths in the I, N, and C phases. The two-dimensional (2D) diffraction patterns were analyzed using the software package, FIT2D, written by Hammersely [11] of European Synchrotron Research Facility. Full width at half-maximum of the diffraction peaks was estimated after background subtraction and used to calculate positional-order correlation lengths of SY aggregates.

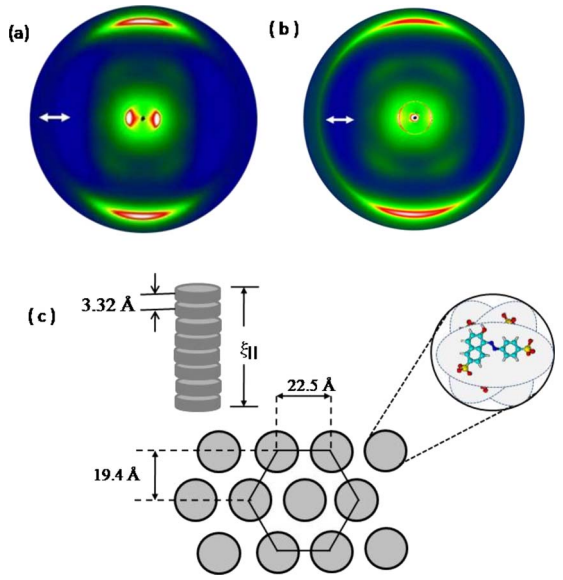

FIG. 4. (Color online) Representative x-ray diffraction pattern in the magnetically aligned (a) N phase of 35 wt % SY+water solution (at 30 °C), and (b) the C phase of 40 wt % SY+water solution (at 30 °C). The inner and outer sharp peaks correspond to *d* values of 24.11 and 3.32 Å in the N, and 19.49 and 3.32 Å in the C phase. In both LC phases, four diffuse intermediate reflections at 5.62 Å are also clearly visible. (c) Schematic representation of hexagonal structure made of columnar stacks in the C phase. The double headed arrows in (a) and (b) represent the direction of the *in situ* magnetic field. The blowup of cylindrical cross section shows a possible stacking of dye molecules with rotation of their planes about the column axis, producing a helical structure [5].

III. RESULTS AND DISCUSSION

The dye SY is an orange-red color powder that easily dissolves in water. Samples held in a 10 μm thick glass cells exhibit characteristic Schlieren or mosaic textures, illustrated in Fig. 2, in the N and C phases [12], respectively. Figures 2(a) and 2(b) show textures in the N phase of the 30 wt % SY solution and the hexagonal C phase of the 40 wt % solution, respectively. The temperature-concentration phase diagram constructed with the help of these results is shown in Fig. 3(a) for SY concentrations ranging from 29 to 40 wt % where the N phase forms. However, the C phase is obtained only for concentrations at or above 40 wt %. The width of the N+I biphasic region is ~10–12 °C. Figure 3(b) represents similar behavior with 1:1 molar ratio of SY: HCl. Evidently, the transition temperatures from the I phase to I+N region and then to the N phase were lowered by ~5–7 °C upon addition of HCl.

Structural characteristics of the nematic and columnar phases are determined from the results of small angle x-ray scattering experiment. Figures 4(a) and 4(b) shows essential features of the diffraction patterns of the two mesophases for the 30 and 40 wt % solution of SY and water, respectively. Three sets of reflections can be seen in these diffraction patterns. One of them is a pair of arcs in the vertical direction, at $d \sim 3.32$ Å, corresponding to the distance between SY molecules within the stack as expected. A second pair of arcs

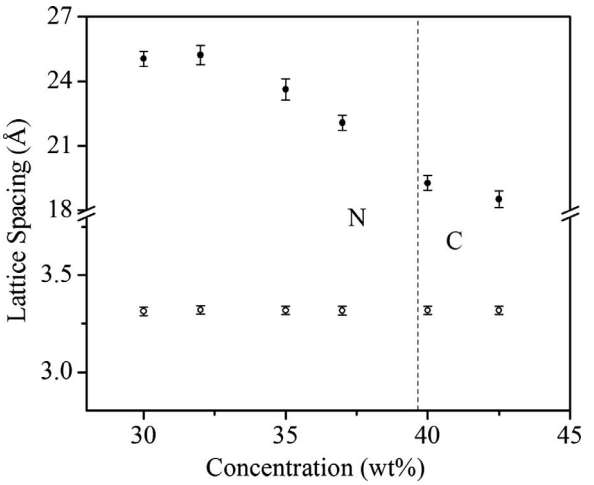

FIG. 5. Variation of interstack (filled circle, top) and intrastack (open circle, bottom) spacing with the concentration of SY+water at room temperature.

seen in the horizontal direction at small angle corresponds to the distance between aggregates, (discussed below). The third set is a group of four faint spots arising from a separation of ~5.6 Å, at ~1:00, 5:00, 7:00 and 11:00 O'clock positions. A faint ring corresponding to these four spots also is visible in the isotropic phase of these solutions. Although the origin of these reflections is unclear, it appears to be related to the structure of dye molecules rather than the organization of aggregates. Edwards *et al.* [5] postulated that alternating π rotation of dye molecules about the aggregate axis is responsible for these reflections. Accordingly, the four peaks may arise from twice the spacing between molecules in a short-pitched chiral arrangement. However, in a field-aligned nematic phase, these peaks and the peaks corresponding to such molecular stacking should be in the same direction. Experimental data are, thus, not in agreement with this explanation [5]. Our results are more consistent with the suggestion of Park *et al.* [13] that these peaks arise from the nonplanar (oblique) orientation of the molecules' phenyl groups/rings with respect to the naphthalene plane in the hydrazone form. As the system enters the C phase, long-range positional order develops in the plane perpendicular to the aggregate axes (nematic director). The small angle arc reflections in the C phase are, in fact, sections of a sharp diffraction ring as seen in Fig. 4(b). Additional faint but narrow peaks are also visible at small angles in Fig. 4(b). Figure 4(c) schematically shows the organization of SY molecules in a column and the hexagonal structure of the C phase. Values of representative intra- and interstack spacings are also illustrated in this figure.

A. Concentration dependence

Concentration dependence of the intra- and intercolumn spacings for SY+water solutions at 30 °C is plotted in Fig. 5. For the range of concentration and temperature covered in this study, the value of intercolumnar separation, corresponding to the Bragg peaks at small angle, varies from ~18 to 25 Å and depends on concentration as previously deter-

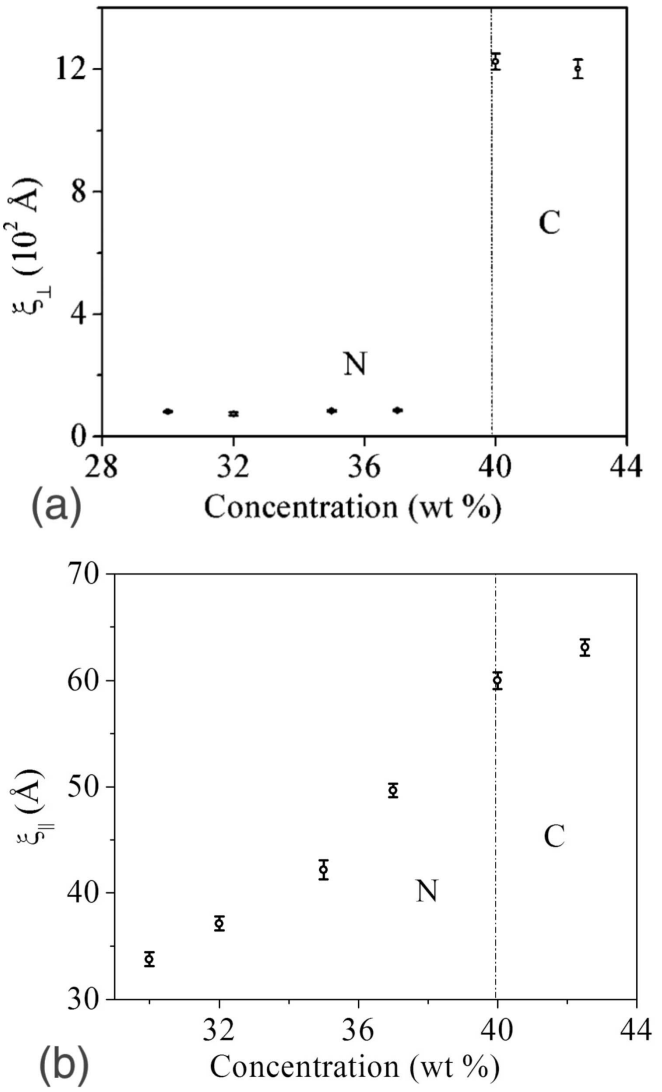

FIG. 6. (a) Transverse positional-order correlation length shows a sharp increase at 40 wt % SY accompanied by the formation of the columnar phase at higher dye concentration, and (b) variation of longitudinal correlation length ($\xi_\parallel$) with concentration.

mined [1,4,13]. The positional-order correlation length transverse to the column axis provides a measure of the distance up to which the intercolumn separation is preserved, or the translational symmetry of the hexagonal lattice is retained. Its value in the C phase is more than an order of magnitude larger than in the N phase, Fig. 6(a), and is limited by the sample mosaicity (i.e., misorientation). The two large-angle diffuse reflections at the meridian positions give a separation of 3.32 ± 0.02 Å between adjacent dye molecules in a column. This is essentially independent of concentration and temperature, as expected.

Longitudinal positional-order correlation length, $\xi_\parallel$, calculated from the width of large-angle peaks, is a direct measure of the height of the aggregates, depicted in Fig. 4(c). Its concentration dependence in the N and C phases is shown in Fig. 6(b). In the N phase, as the concentration increases from 30 to 37 wt %, the height of the aggregates grows from about 34 to 50 Å corresponding to ~10 to 15 molecules per aggregate. This agrees with the results of Luoma [4] that the aggregation starts at low concentration and continues to grow with concentration as revealed in their birefringence measurements. In fact, we find that $\xi_\parallel$ is substantial (24 Å) even in the isotropic phase at 25 wt % concentration. The minimum aggregate height at which the N phase begins to form is about 34 Å, or 10 SY molecules, in agreement with Park *et al.* [13]. The results further show that the optimum aggregate length necessary to form the C phase is ~60 Å which contains 18 molecules. This aggregation process is believed [2] to be "isodesmic," in that, the addition/removal of one molecule to a stack is associated with the same increment/decrement of free energy [2] with changing concentrations. The aggregate length grows by roughly three molecules and the rate of aggregate growth with concentration apparently changes across the N to C phase transition.

TABLE I. Lattice parameter a and radius r of columns in the C phase of SY.

Conc. (wt %)	φ	d (Å)	a (Å)	r (Å)
40.0	0.32	19.49 ± 0.35	22.51 ± 0.40	6.714 ± 0.12
42.5	0.35	18.77 ± 0.39	21.67 ± 0.45	6.689 ± 0.14

The x-ray scattering pattern of the C phase consists of Bragg peaks corresponding to lattice spacings of 19.5, 11.2, 9.8, and 7.4 Å which are in the approximate ratios of $1:\sqrt{3}:\sqrt{4}:\sqrt{7}$, and confirm its hexagonal structure. The position q_0 of the first peak is related to the distance between the centers of adjacent columns by $a=(2/\sqrt{3})2\pi/q_0$. Geometrical relations [14–16] allow us to relate the effective radius of the columns, r, to the lattice parameter, a, and the volume fraction φ of SY using

$$r = a\left(\frac{\sqrt{3}\varphi}{2\pi}\right)^{1/2}.$$

The volume fraction of SY used here was calculated from the weight concentration in a manner consistent with that of Tiddy *et al.* [17]. The effective radius of the aggregates was calculated to be ~6.7 Å as shown in Table I. It indicated that the size of the rodlike aggregates was same as molecular lateral dimension (see Fig. 1).

The area of cross section of cylindrical column of SY aggregate calculated using the values of r is comparable to the area of cross section of SY molecule leading us to conclude that the SY aggregates are unimolecular stacks as previously reported [1,2,5,13] and not chimney-like structures.

B. Temperature dependence

The effect of temperature on the inter- and intrastack spacings in the N and C phases of SY solutions is shown in Fig. 7. The phase boundaries, primarily based on optical texture observations, are indicated by vertical broken lines for

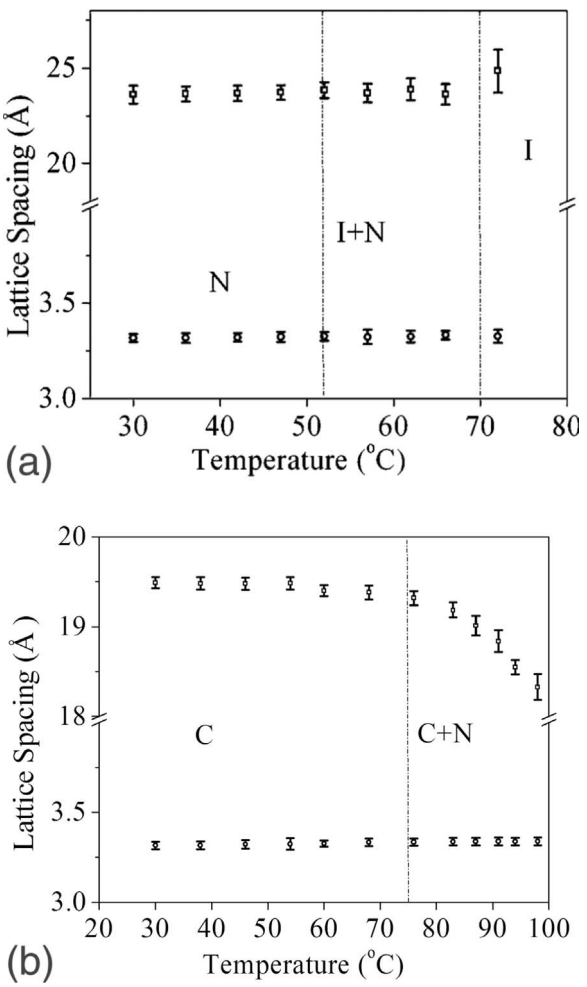

FIG. 7. Temperature dependence of (□) inter- and (○) intrastack spacing in (a) the N phase (35 wt %), and (b) the C phase (40 wt %).

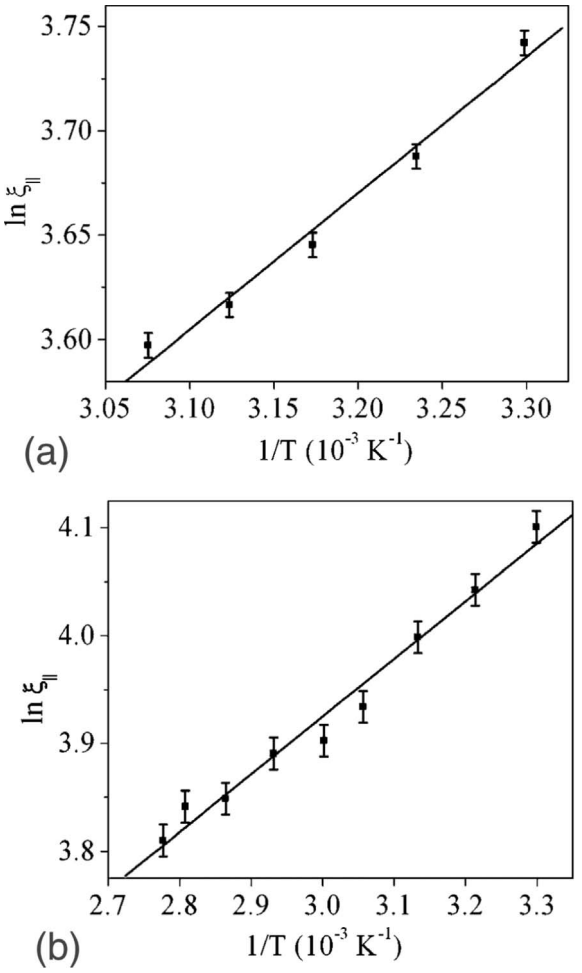

FIG. 8. Variation of longitudinal correlation length, $\xi_{\|}$, with temperature in the (a) N phase of 35 wt % SY+water solution and (b) the C phase of 40 wt % SY+water solution.

clarity. In the N phase, no obvious change in the interstack spacing is seen. It varies somewhat in the biphasic region (N+I) and appears to increase in the isotropic (I) phase, Fig. 7(a). In the C phase, Fig. 7(b), the interstack spacing does not exhibit strong temperature dependence. However, in the (C+N) region, it decreases with temperature. This is understandable in term of changing average aggregate height as one enters the biphasic region. In the biphasic region, the system is partially in the N phase, in which the aggregates become shorter. Consequently, the number of stacks per unit volume increases bringing them closer to each other and resulting in the observed decrease of interstack spacing.

The positional-order correlation length, $\xi_{\|}$, is calculated as a function of temperature for two concentrations of SY, Fig. 8. It is found to be strongly dependent on concentration as evident from a comparison of the values of correlations in Figs. 8(a) and 8(b) for the 35 and 40 wt % solutions, respectively. The linearity of the plot of $\ln \xi_{\|}$ vs $1/T$ (K^{-1}) reveals an Arrhenius behavior [18], described by the fits to the equation,

$$\xi_{\|} = \xi_0 \exp\left(\frac{E}{2k_B T}\right),$$

where ξ_0 represents the asymptotic value of the $\xi_{\|}$. This expression for correlation length comes from a simple calculation based on energy and entropy consideration from which the average number of molecules per aggregate can be calculated [19]. Linear fits to the data, shown as solid straight lines in Fig. 8, yield values of the activation energy E (or, scission energy, i.e., the energy needed to split an aggregate into two), $E=4.3\pm0.3k_BT$ (1.8×10^{-20} J) for the N phase (35 wt %) and $E=3.5\pm0.2k_BT$ (1.5×10^{-20} J) for the C phase (40 wt %). The value of the bare correlation length, ξ_0, are 4.86 ± 1.16 Å and 10.16 ± 1.09 Å in the N and C phases, respectively. Here, K_B and T represent the Boltzmann constant and absolute temperature, respectively. These values are much smaller than the room temperature stacking/scission energy of $\sim 7k_BT$ previously determined [1,2,13] from spectral changes as a function of concentration. The difference between our values of E and those previously reported [1] is not surprising because UV absorption measure-

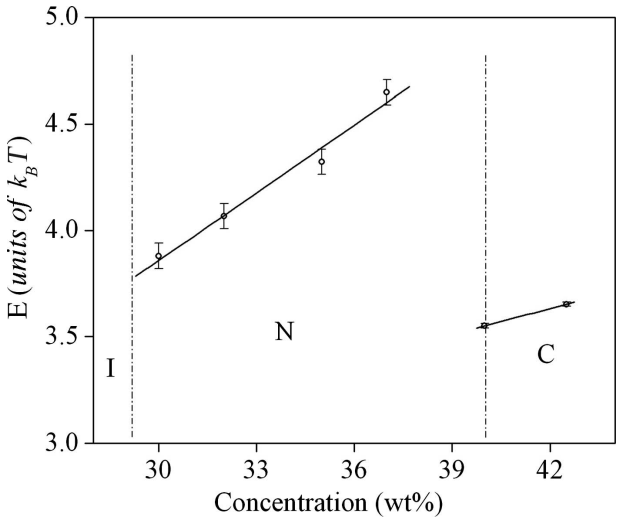

FIG. 9. The scission energy, E, shown as a function of SY concentration. Values of E are calculated from the parallel correlation length measured at room temperature, and using the bare correlation length, ξ_0, of 4.86 and 10.16 Å in the N and C phases, respectively.

ments in reference [1] were made in solutions of ~45 times smaller concentration.

The scission energy estimated for different concentrations, using room temperature measurements and the calculated bare correlation length of 4.86 and 10.16 Å in the N and C phases, is plotted in the Fig. 9. Here, we have assumed the bare correlation length to remain independent of concentration within a mesophase, which remains to be experimentally tested. Nevertheless, it provides a way to qualitatively determine the concentration dependence of E. The result not only illustrates the concentration dependence of E within each phase but also reveals that the rate of change (slope) of E is different in the two mesophases. A more accurate estimation of the concentration dependence of E can be obtained from direct measurements of thermal evolution of longitudinal correlation lengths for various concentrations. Such experiments will be conducted in near future. It appears counterintuitive to obtain a lower value of E in the C phase that has longer aggregates than the N phase with higher E. However, it is conceivable to obtain longer aggregates at higher (concentrations) availability of monomers even with lower scission energy. Understanding the process responsible for the reduction of E in the C phase remains a subject for future experimental and theoretical investigations.

The scission energy of a charged system of molecules that undergoes cylindrical aggregation is reduced by an amount E_e due to dissociation of SY molecules which produce aggregates with surface charge density and releases Na^+ counter ions into the solvent. Mutual electrostatic repulsion between charged monomers mediated by the counterion cloud [20] determines the value of E_e. As the volume fraction of SY increases, a larger number of counterions is released into a smaller volume of solvent, thereby increasing their density. This has the net effect of decreasing the electrostatic repulsion between monomers and between the aggregates. Evidently, addition of ionic solute is expected to influence transition temperatures and E_e.

C. Effect of ionic additive

In the absence of added salt, the screening length, R_B, is essentially the separation between aggregates and it varies as $\sim 1/\sqrt{\varphi}$ with concentration. The electrostatic energy E_e can be calculated using the formula [20–24],

$$E_e = l_B v^{*2} r k_B T/\sqrt{\varphi}.$$

Here, $l_B (=e^2/4\pi\varepsilon\varepsilon_0 k_B T)$ is the Bjerrum length [13] defined as the distance at which electrostatic repulsion between two charges in a medium becomes comparable to the thermal energy $k_B T$, ε is the dielectric constant of the medium (water), ν^* is the effective linear charge density, and r is the effective radius of the aggregate.

Since the formation of SY aggregates is mediated by electrostatic interactions, it is profoundly affected by changes in the concentrations of ions in the solution. To quantitatively understand this dependence, we added HCl in different molar ratios with respect to SY and determined the resultant changes in the aggregate size, shape, and organization in the two liquid crystal phases.

The correlation length $\xi_\parallel$ decreases at all temperatures for, both, 35 and 40 wt % solutions when *HCl* is added (Fig. 10). The filled points (on top) in Fig. 10 correspond to SY +water solutions whereas the unfilled points (bottom) represent solutions with HCl: SY in 1:1 molar ratio. The aggregates became shorter when HCl was added lowering phase boundaries by about 4–5 °C, as shown in the phase diagram [Fig. 3(b)]. A significant drop in $\xi_\parallel$, of magnitude between ~24 and 43 Å, is observed across the five; C, N+C, N, (N+I) and I; regions. Approximate number of molecules per aggregate is 11 in the N phase, 8 in the (I+N) biphasic region, and 6 molecules in the I phase of the 35 wt % solution. The number of molecules per aggregate for 40 wt % solution, Fig. 10(b), is ≥ 12 in the C phase and ≥ 8 in the biphasic N+C region. Addition of HCl lowers the *p*H of the solution. A measurement, using a *p*H meter, performed in 30 wt % solution without and with HCl indicated a decrease from 7.8 ± 0.1 to 0.5 ± 0.1. With increased H^+ concentration, the aggregate size is expected to increase due to stronger binding (i.e., less electrostatic repulsion) between monomers. However, the observed decrease in aggregation number suggests that other factor may be responsible for disaggregation. One possibility is the dominant conformation of SY molecule which changes from azo tautomer to hydrazone tautomer at low *p*H values. This is likely to lower the molecular aggregation as fewer π electrons (i.e., smaller flat-core) become available in more acidic solutions [25–28]. A comparison of the data displayed in Figs. 7(a) and 11, shows that the column-column separation and the separation between molecules in an aggregate remains the same within experimental uncertainties.

In order to better understand the effect of ionic additive on column aggregation, a systemic study was conducted on solutions with different molar ratios of HCl: SY, at 30 and 40 wt % concentrations. It should be pointed out that the dye sample used in this part of the study was recrystallized at a different time. It appears to have somewhat different purity. Consequently, the values of correlation lengths in this set of experiments are somewhat different than reported earlier.

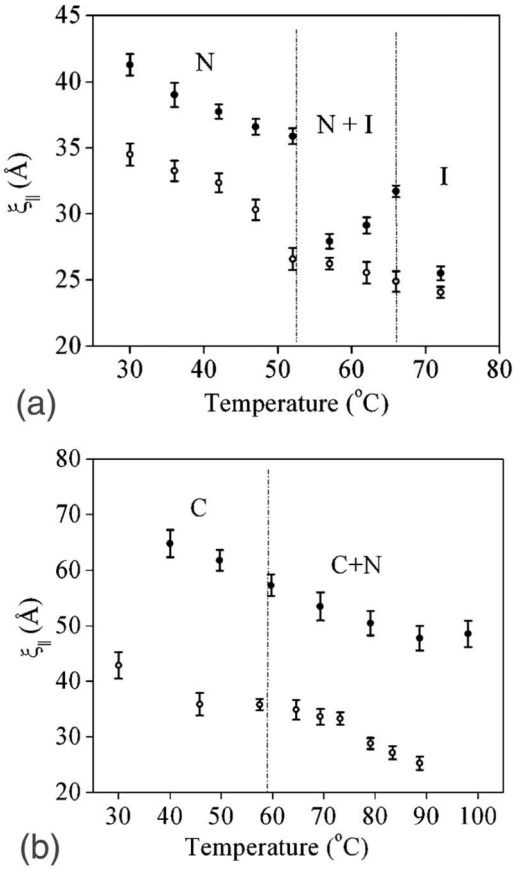

FIG. 10. Variation of $\xi_{\parallel}$, with temperature in SY solutions without (filled points, top) and with (unfilled points, bottom) HCl (in 1:1 mol ratio) in (a) the N (35 wt %) and (b) the C phases (40 wt %).

The conclusions drawn from these data about the relative changes induced by different concentration of HCl provide a useful insight into the underlying mechanisms. The results, i.e., the values of $\xi_{\parallel}$, are presented in Figs. 12(a) and 12(b) in the N, N+C, and C phase regions. It is clear that the number of molecules per aggregate decreases linearly from ~11 to 8

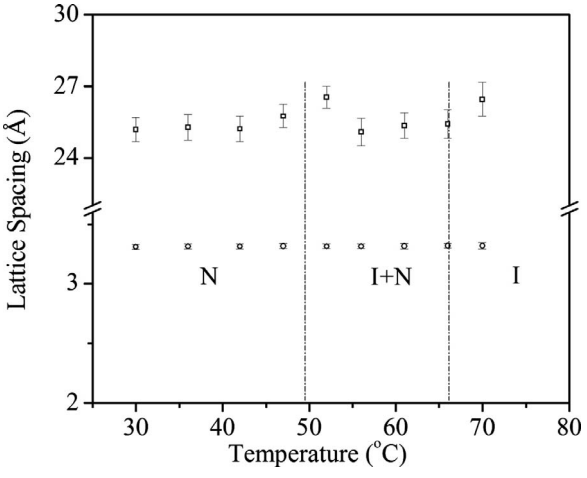

FIG. 11. Variation of interstack (□, on top) and intrastack (○, bottom) spacing with temperature in the N phase of (35 wt %) solutions in water with 1:1 mol ratio of HCl and SY.

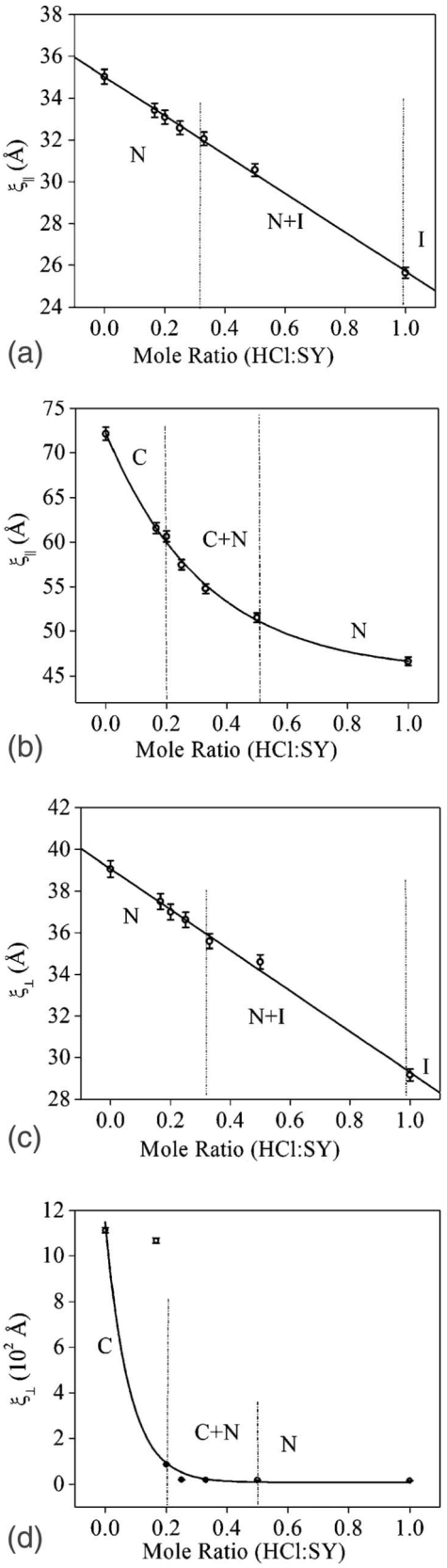

FIG. 12. Variation of $\xi_{\parallel}$ for solution of SY and HCl dissolved in water in (a) the N phase of 30 wt % (b) the C phase of 40 wt % solutions. Variation in the transverse correlation length in (c) the N phase of 30 wt %, and (d) the C phase of 40 wt % solutions.

in the N phase of the 30 wt % solution [Fig. 12(a)] with increasing HCl. For the 40 wt % solution, this number changes from >21 [in the C phase, Fig. 11(b)] to 18–15 in the (C+N) region and to ~14 in the N phase. This decrease of aggregates' length with the addition of HCl leads one to conclude that higher concentration of ionic dopants aids in the dissociation of dye aggregates. The distances over which positional order of aggregates in the N and C phases persists in the transverse direction is shown in Figs. 12(c) and 12(d). The perpendicular correlation length, $\xi_{\perp}$, also decreases with the mole ratio. Figure 12(d) further shows that positional-order correlations in the C phase extend to a length scale that is at least one order of magnitude larger than the N phase, as expected.

IV. CONCLUSIONS

From the values of intermolecular separation (3.32 Å), which is characteristic of π-π stacking, and aggregate diameter (13.4 Å) that is comparable to the dimension of dye molecules (13.7 Å), it is affirmed that the SY aggregates are unimolecular. The four weak x-ray spots observed at intermediate angles suggest that the structure of SY aggregates is not simple rod-shaped stacks. An experimental investigation to find the source of these reflections is currently in progress. In addition to determining the concentration and temperature dependences of the structure of nematic and columnar phases, we measured the growth of the aggregates and the (correlation) length scale over which positional-order correlations prevail in the direction perpendicular to the nematic director. The scission energy of SY aggregates, determined from the change of $\xi_{||}$ with temperature, is found to be $4.3 \pm 0.3 k_B T$ and $3.5 \pm 0.2 k_B T$ in the nematic and columnar phases, respectively. The concentration (and phase) dependence of E clearly shows that the aggregation process is not isodesmic. These values of the scission energy E are smaller than previously published and stronger electrostatic effects at the higher concentration used in this study may be responsible for the difference. No dramatic changes in intra- and interstack spacings are observed when solution pH is altered by adding HCl. However, addition of HCl lowers transition temperatures and causes a significant drop in the longitudinal correlation length, $\xi_{||}$, in the N and the C phases underscoring the role electrostatic interactions play in these systems.

ACKNOWLEDGMENTS

This research was supported, in part, by National Science Foundation's Materials World Network Grant No. DMR-0806991. Use of the Advanced Photon Source (APS) was supported by the U.S. Department of Energy, Basic Energy Sciences, Office of Science, under Contract No. W-31-109-Eng–38. The Midwest Universities Collaborative Access Team (MUCAT) sector at the APS is supported by the U.S. Department of Energy, Basic Energy Sciences, Office of Science, through the Ames Laboratory under Contract No. W-7405-Eng-82. We thank Douglas Robinson for the beamline management and valuable support during the experiments, and Mohan Srinivasarao and Oleg Lavrentovich for helpful discussions.

[1] V. R. Horowitz, L. A. Janowitz, A. L. Modic, P. A. Heiney, and P. J. Collings, Phys. Rev. E **72**, 041710 (2005).
[2] J. Lydon, Curr. Opin. Colloid Interface Sci. **8**, 480 (2004).
[3] H. von Berlepsch, C. Böttcher, and L. Dähne, J. Phys. Chem. B **104**, 8792 (2000).
[4] R. J. Luoma, Ph.D. dissertation, Brandeis University, 1995.
[5] D. J. Edwards, J. W. Jones, O. Lozman, A. P. Ormerod, M. Sintyureva, and G. J. T. Tiddy, J. Phys. Chem. B **112**, 14628 (2008).
[6] Yu. A. Nastishin, H. Liu, T. Schneider, V. Nazarenko, R. Vasyuta, S. V. Shiyanovskii, and O. D. Lavrentovich, Phys. Rev. E **72**, 041711 (2005).
[7] A. P. Ormerod, Ph.D. thesis, University of Salford, 1995.
[8] S. Mohanty, S. -H. Chou, M. Brostrom, and J. Aguilera, Mol. Simul. **32**, 1179 (2006).
[9] J. N. Israelachvili, *Intermolecular and Surface Forces*, 2nd ed. (Academic Press, London, 1992).
[10] J. E. Lydon, Mol. Cryst. Liq. Cryst. Lett. **64**, 19 (1980).
[11] A. P. Hammersley, S. O. Svensson, M. Hanfland, A. N. Fitch, and D. Hausermann, High Press. Res. **14**, 235 (1996).
[12] I. Dierking, *Textures of Liquid Crystals* (Wiley-VCH GmbH & Co. KGaA, Weinheim, 2003).
[13] H.-S. Park, S.-W. Kang, L. Tortora, Y. Nastishin, D. Finotello, S. Kumar, and O. D. Lavrentovich, J. Phys. Chem. B **112**, 16307 (2008).
[14] C. Ruslim, D. Matsunaga, M. Hashimoto, T. Tamaki, and K. Ichimura, Langmuir **19**, 3686 (2003).
[15] L. Ramos and P. Fabre, Langmuir **13**, 682 (1997).
[16] L. Q. Amaral, A. Gulik, R. Itri, and P. Mariani, Phys. Rev. A **46**, 3548 (1992).
[17] G. J. T. Tiddy, D. L. Mateer, A. P. Ormerod, W. J. Harrison, and D. J. Edwards, Langmuir **11**, 390 (1995).
[18] Yu. A. Nastishin, H. Liu, S. V. Shiyanovskii, O. D. Lavrentovich, A. F. Kostko, and M. A. Anisimov, Phys. Rev. E **70**, 051706 (2004).
[19] P. van der Schoot and M. E. Cates, Langmuir **10**, 670 (1994).
[20] M. E. Cates and S. J. Candau, J. Phys.: Condens. Matter **2**, 6869 (1990).
[21] F. C. Mackintosh, S. A. Safran, and P. A. Pincus, Europhys. Lett. **12**, 697 (1990).
[22] R. M. Fuoss, A. Katchalsky, and S. Lifson, Proc. Natl. Acad. Sci. U.S.A. **37**, 579 (1951).
[23] A. G. Zilman and S. A. Safran, Phys. Rev. E **66**, 051107 (2002).
[24] I. Couillet, T. Hughes, G. Maitland, F. Candau, and S. J. Candau, Langmuir **20**, 9541 (2004).
[25] A. Stroobants and H. N. W. Lekkerkerker, Macromolecules **19**, 2232 (1986).
[26] V. Srinivasan and D. Blankschtein, Langmuir **19**, 9946 (2003).
[27] S.-W. Tam-Chang, J. Helbley, and I. K. Iverson, Langmuir **24**, 2133 (2008).
[28] S. K. Prasad, G. G. Nair, G. Hegde, and V. Jayalakshmi, J. Phys. Chem. B **111**, 9741 (2007).